# Analysis of elastic nonlinearity using the scaling subtraction method

C. L. E. Bruno,[1,2,*] A. S. Gliozzi,[1,†] M. Scalerandi,[1,‡] and P. Antonaci[2,§]
[1]*Physics Department, Politecnico di Torino, Corso Duca degli Abruzzi, 24-10129 Torino, Italy*
[2]*Structural Engineering Department, Politecnico di Torino, Corso Duca Degli Abruzzi, 24-10129, Torino, Italy*
(Received 24 July 2008; revised manuscript received 14 January 2009; published 18 February 2009)

Analyzing the nonlinear part of a signal generated by the response of a sample to an elastic excitation is a powerful tool to gain information on the material microstructure, including the presence of damage. Analysis using band-pass filtering or equivalent methods is often difficult due to the low amplitude of the harmonics contained in the signal. This is the case for the detection of early damage in granular samples with damage induced by a quasistatic loading, as analyzed in this paper. An experimental study, based on the scaling subtraction method, is presented here, showing the possibility of monitoring the variation in the sample nonlinearity during the evolution of damage and allowing linking it to different physical processes. The efficiency of the method in eliminating nonlinear contributions due to the experimental setup is proved through a numerical analysis.

DOI: 10.1103/PhysRevB.79.064108 PACS number(s): 43.25.+y, 81.70.Cv, 43.35.+d

## I. INTRODUCTION

The presence of nonlinear terms in the elastic response of a granular medium to a wave excitation is considered a microstructure indicator related to the presence of microcracks.[1–6] Depending on the modality of the experiment, features such as higher-order harmonics,[7] subharmonics,[8] or sidebands[9] are known to provide an indication of the interaction between the injected wave and the nonlinear scatterers present in the sample. A very sensitive nonlinear contribution may be identified in the attenuation as well.[10,11]

Many methods have been presented in the past to extract nonlinear features from the elastic response of a specimen impinged by an ultrasonic wave, in particular band-pass filtering,[3,12,13] classical fast Fourier transform (FFT) analysis[14–17] and phase-coded subtraction methods.[18] All of the above-mentioned methods consider only part of the nonlinear signature, in general, that is due to higher-order harmonics or sidebands, excluding therefore the contribution observable at the fundamental frequency. As a result, in particular when dealing with early/small damage, these methods need very accurate measurements to be performed in a controlled environment. In fact, the features to be extracted have a small amplitude (few percent of the recorded signals), and the nonlinear contribution to the signal decay rapidly when moving far from the nonlinearity source. As a result, the signature of the nonlinear scatterers can easily fall below the noise level.

At the state of the art, nonlinear ultrasonic measurements are not easy to perform for solid samples, in which different sources of nonlinearity can be present at the same time. In particular, measurements can be easily contaminated by the nonlinearity intrinsic in the acquisition system, which poses serious limits in the voltage amplitudes that can be used in experiments. An accurate testing of the linear limit of transducers, electronics, and power amplifier must always be performed to define *a priori* the maximum upper voltage level.

Proven that the acquisition system is linear, any break in proportionality between the input and the output can be totally associated to the nonlinear elastic elements in the sample. This can be due to different causes which can be grouped into three main classes of phenomena:

(1) amplitude dependence of the elastic constants and, consequently, of the wave speed, which causes changes in the phases of the recorded signal;

(2) nonlinear attenuation mechanisms, which influence the amplitude of the recorded signal;

(3) nonlinear coupling in the wave equation, which allows the generation of higher-order harmonics, sidebands, or subharmonics.

It is interesting to note that filtering methods only capture the last of the three mechanisms. On the opposite, amplitude effects on attenuation and wave speed have influence mostly on the component of the signal at its fundamental frequency, resulting, e.g., in a shift of the resonance frequency with the excitation amplitude. Extracting these three contributions from a single signal is important for a better understanding of the mechanisms involved when the nonlinearity is generated.

To this purpose, a valid alternative to the traditional filtering techniques is given by the scaling subtraction method (SSM), which consists of a simple difference between signals once a reference signal has been defined for the examined sample.[11] Besides the advantage of not needing parameters for the analysis (e.g., number of periods, sampling rate, etc) which are influent for a successful filtering approach, the SSM analysis also accounts for nonlinear attenuation and phase delays in the recorded signals, i.e., nonlinear effects at the fundamental frequency. These effects have been shown to be much stronger than those on harmonics (at least in granular samples such as concrete).[11] It follows that the analysis can be easily conducted in a narrow frequency band, with obvious advantages from the point of view of the choice of the transducers to be used.

We show in this paper that by using the SSM approach as it will be presented in Sec. II, we can extract information on the nonlinearity (and its evolution) from experimental data and correlate this information to the presence of an underlying microstructure. The signals recorded by a transducer can be analyzed in order to provide four nonlinearity indicators,

 

each sensible to a different microfeature (Sec. III). In Sec. IV, a discussion is presented through numerical examples to indicate how the method and the separation of the effects can support the solution of problems emerging in different applications of ultrasound in damage diagnosis. In particular, we prove that the SSM approach can be used to separate physical nonlinear signatures from the artifacts due to the measurement system, such as equipment nonlinearity or noise.

## II. THEORY

### A. Scaling subtraction method

Propagation of elastic waves in a nonlinear medium (or in a portion of it) is governed by a nonlinear stress-strain constitutive equation. In general, for a one-dimensional wave propagating in a nonlinear elastic medium with hysteresis, the stress-strain equation (constitutive law) can be obtained by the expansion of the elastic strain energy in powers of the strain tensor, with additional contributions due to hysteresis. Of course, different equations can be used to model different types of nonlinearity: classical nonlinear models,[19] hysteretic models,[20–23] bond models,[24] elastoplastic models,[25] etc.

Given the material constitutive law, the equation of motion can be obtained as

$$\rho\frac{\partial^2\epsilon}{\partial t^2} = \frac{\partial^2\sigma}{\partial x^2} + f(x,t), \tag{1}$$

where $\rho$ is the medium density, $\sigma$ is the stress, $\varepsilon$ is the strain, and the function $f$ defines the source.

The nonlinear contributions in the stress-strain relation break the proportionality between the excitation (defined by $f$) and the response. Note that nonlinear contributions rise only if a high amount of energy is injected in the sample. In this case the superposition principle is violated. The SSM exploits the loss of scaling properties of the recorded signals.

To explain the procedure, we start considering that in most cases the elastic response of the excited medium to an elastic wave can be expressed as a superposition of cosinusoidal waves. Formally, given a pure tone excitation with amplitude $A$ and frequency $\omega_0$, when stationary conditions are reached, the received signal $v_A(t)$ can be expressed as

$$v_A(t) = \sum_{n=1}^{\infty} B_n(A)\cos[n\omega_0 t + \varphi_n(A)]. \tag{2}$$

The response amplitudes $B_n(A)$ are governed by an amplitude-dependent damping $\gamma(A)$. For simplicity, the frequency dependence of the damping is neglected in this discussion. Note that also phases of each harmonic contribution in the summation are a function of the amplitude.

In order to separate the nonlinear signature in signals in the form of Eq. (2), a linear "reference signal" is needed, which represents the linear response associated to an equivalent linear (undamaged) medium. The definition of such a "reference" is not trivial since it must be defined with an experimental procedure on the same sample (without changing the coupling of the transducers). It must correspond to the linear (ideal) response at the very same amplitude $A$. Being the nonlinear signature a small effect, in particular for early damage, defining a physical reference specimen identical (except for nonlinearity) to that analyzed is completely unfeasible.

Let us then consider that in the limit of small excitations the strain is small and nonlinear contributions in the stress-strain equation are negligible. It follows that the system is described by a linear wave equation. Thus, when the sample is excited with a sufficiently low amplitude $A_{\text{lin}}$, the resulting recorded signal does not contain higher-order harmonics,

$$v_{\text{lin}}(t) = B_1(A \to 0)\cos(\omega_0 t + \varphi_0). \tag{3}$$

Without loss of generality and for simplicity of notation, in the following we will assume $\varphi_0=0$.

Once measured $v_{\text{lin}}(t)$, the reference signal at amplitude $A=kA_{\text{lin}}(k \gg 1)$ can be defined in a post processing procedure. In fact, if the system was linear, the superposition principle would hold and the output signal would be expected to be

$$v_{\text{ref}}(t) = kv_{\text{lin}}(t) \neq v_A(t). \tag{4}$$

In the following, $v_{\text{ref}}(t)$ will be assumed as the linear "reference."

The SSM defines the nonlinear response of the specimen through the scaled subtracted signal (SSM signal)

$$w_A(t) = v_A(t) - v_{\text{ref}}(t), \tag{5}$$

where the signal $v_A(t)$ is a high-amplitude $(A=kA_{\text{lin}})$ signal, which can be expressed in the form of Eq. (2). From Eqs. (3) and (4) we obtain

$$w_A = -kB_1(A_{\text{lin}})\cos(\omega_0 t) + B_1(A)\cos[\omega_0 t + \varphi_1(A)] + \sum_{n=2}^{\infty} B_n(A)\cos[n\omega_0 t + \varphi_n(A)]. \tag{6}$$

Of course $w_A(t)$ vanishes (except for noise effects) if the material is perfectly linear.

Given a material model based on the classical Landau theory, it is possible to extract the well-known $\beta$ and $\delta$ parameters[26] from the SSM signal $w_A(t)$, at least in principle. An example of derivation is reported in the Appendix. This issue is not further investigated here since, in our opinion, the nonlinearity of the samples studied in this paper is not of the classical type, but on the contrary, the cause of the nonlinear behavior of the specimen is mainly due to hysteresis[1] or transitions to nonequilibrium states[21,27,28].

From the SSM signal $w_A(t)$, we can define a quantitative parameter $\theta(A)$ to represent and quantify the nonlinear signature of the investigated sample. The parameter, which from now on will be called the SSM indicator, has been defined as the "energy" of the SSM signals $w_A(t)$,

$$\theta(A) = \frac{1}{nT}\int_0^{nT} w_A^2(t)dt. \tag{7}$$

Of course, $\theta(A)$ is dependent on the amplitude of the large excitation used in the analysis, as will be discussed in the results (Sec. II D).

The scaling subtraction method has the advantage with respect to FFT analysis or similar approaches that the nonlinear signature is derived by a simple subtraction method and without the introduction of mathematical parameters, usually present in the filtering procedures (e.g., time window length, zero padding, etc.). We also remark that, for an experimental procedure based on SSM, recorded signals must be triggered and synchronized in order to avoid any effect caused by measurement delays.

### B. Properties of the SSM signals

Three contributions in the SSM signal can be distinguished, corresponding to the three sources of nonlinearity previously introduced. From Eq. (6), simple trigonometric calculations indicate that $w_A(t)$ can be written as

$$w_A(t) = w_1(t) + w_2(t) + w_3(t), \tag{8}$$

where

(i) $w_1(t)=2kB_1(A_{\text{lin}})\cos(\omega_0 t+\frac{\varphi_1(A)}{2})\cos(\frac{\varphi_1(A)}{2})$ is the nonlinear contribution due to the phase $\varphi_1$ of the component at the fundamental frequency $\omega_0$. It only depends on the (linear) "reference signal" amplitude $B_1(A_{\text{lin}})$. The energy of such signal can be defined, equivalently to what reported in Eq. (7), as the phase nonlinear indicator

$$\theta_1 = 2k^2B_1^2\cos^2\left(\frac{\varphi_1(A)}{2}\right). \tag{9}$$

In a given material the phase of a wave is related to the wave speed and to the length of the traveled path, which in this case remains constant (except for a second-order term due to changes in the attenuation). Assuming the material to be nondispersive, the velocity is directly related to the bulk modulus $K$ through the relation $v=\sqrt{\frac{K}{\rho}}$. Thus $\theta_1$, which depends on the phase of the large amplitude signal only, reflects a *variation in the stiffness* of the medium when excited at the amplitude $A$, with respect to the stiffness when the material is excited at amplitude $A_{\text{lin}}$. Less often a variation in velocity can be related to a variation in density. Note that the idea remains valid also in the case of dispersive media, being the phases evaluated at fixed input frequency.

(ii) $w_2(t)=[B_1(A)-kB_1(A_{\text{lin}})]\cos[\omega_0 t+\varphi_1(A)]$ is the nonlinear contribution due to nonlinear attenuation. It depends on both the (linear) reference signal amplitude and the higher amplitude. Since nonlinear attenuation increases with amplitude, we always expect the amplitude of the scaled linear signal to be slightly higher than that of the high-amplitude signal, except for effects related to the shift of the resonance curve of the specimen. The corresponding nonlinear attenuation indicator is

$$\theta_2 = \frac{1}{2}[B_1(A) - kB_1(A_{\text{lin}})]^2. \tag{10}$$

The indicator $\theta_2$ exploits the dependence of the *attenuation coefficient* $\gamma(A)$ on the amplitude. The origin of nonlinear attenuation is likely to reside in a combination of several effects, mainly spectral broadening, hysteresis, and resonance frequency shift (usually negligible). To date, it is hard to isolate each single contribution and to link attenuation to nonlinear parameters, such as beta or delta. A specific analysis using broadband transducers might allow providing evidence of the link between energy transferred to higher-order harmonics and loss of energy due to attenuation.

(iii) $w_3(t)=\Sigma_{n=2}^{\infty}B_n(A)\cos[n\omega_0 t+\varphi_n(A)]$ represents the contribution of higher-order harmonics. It corresponds to signals defined using band-pass filtering and a corresponding harmonics indicator $\theta_3$ can be introduced as well. It contains information on the nonlinear and hysteretic parameters of the wave equation.

The first two contributions highlight how part of the stronger nonlinear feature resides at the fundamental frequency. When the fundamental frequency is omitted from the analysis of the signals (e.g., by band-pass filtering), the stronger nonlinear effects are neglected.

### C. Experimental separation of the $w_i(t)$ contributions

Given an experimental set of data, the three components $w_i(t)$ can be individually analyzed. We discuss here a method to separate the three individual signals $w_i(t)$ $(i=1,2,3)$ from the total SSM signal $w_A(t)$, given *only* the measured experimental signals $v_A(t)$ and $v_{\text{lin}}(t)$.

To this purpose we first derive three intermediate signals from $v_A(t)$:

(a) $v_A'(t)$: the original signal $v_A(t)$ is filtered around the fundamental frequency (band-pass filter $0.5\omega_0<\omega<1.5\omega_0$). The result is normalized to the same amplitude of the reference signal $[v_{\text{ref}}=A/A_{\text{lin}}v_{\text{lin}}(t)]$. It follows that, assuming the experimental signals approximately corresponding to those theoretically expected from Eqs. (2) and (3), $v_A'(t)=kB_1(A_{\text{lin}})\cos[\omega_0 t+\varphi(A)]$. Therefore $w_1(t)=v_A'(t)-v_{\text{ref}}(t)$.

(b) $v_A''(t)$: the original signal $v_A(t)$ is filtered around the fundamental frequency (band-pass filter $0.5\omega_0<\omega<1.5\omega_0$). The resulting signal is phased with the reference signal, i.e., $v_{\text{ref}}(t)$ is shifted in time to obtain maximum correlation with $v_A(t)$. Assuming the experimental signals to approximately correspond to those theoretically expected from Eq. (3), the shift corresponding to maximum correlation is $\Delta t=\varphi_1(A)/\omega_0$ and $v_A''(t)=B(A)\cos[\omega_0(t-\Delta t)+\varphi_1(A)]=B(A)\cos(\omega_0 t)$. Therefore $w_2(t)=v_A(t)-v_A''(t)$.

(c) $v_A^F(t)$: the original signal $v_A(t)$ is high-pass filtered $(1.5\omega_0<\omega<7.5\omega_0)$. It follows that $w_3(t)=v_A^F(t)$.

### D. Results

To illustrate the procedure to define the SSM signal and to separate the three independent contributions, we analyze here a given set of two experimental signals obtained by exciting a nonlinear mortar sample with a sinusoidal wave at frequency $\omega_0$. The experimental signals used in this paragraph are obtained in the same experimental conditions of those described in Sec. III, therefore, we postpone the description of the experimental setup to Sec. III A.

A linear signal $v_{\text{lin}}(t)$ has been measured, corresponding to the output generated by a low input amplitude excitation ($A_{\text{lin}}=4$ Volts) and a nonlinear signal $v_A(t)$, resulting from a higher input amplitude ($A=20$ Volts). The two have been recorded once stationary conditions have been reached. The

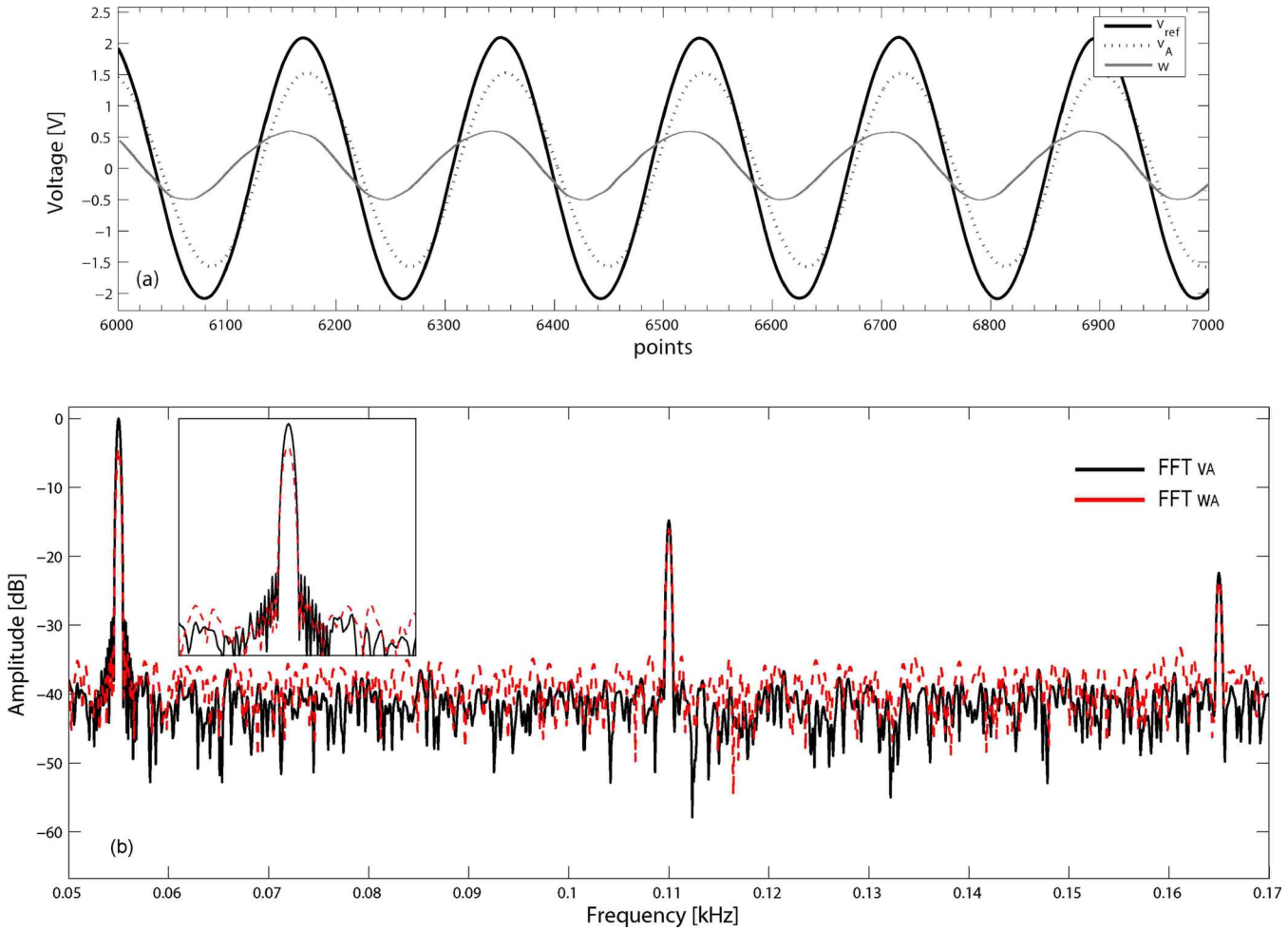


FIG. 1. (Color online) SSM signal. (a) Superposition of the linear reference signal $v_{\mathrm{ref}}$ (solid line) on the nonlinear signal $v_A$ (dotted line). The SSM signal $w$ is also reported; $w$ is given by the difference of the reference and nonlinear signals. (b) FFT of the nonlinear signal $v_A$ (solid black line) and of the SSM signal $w$ of Fig. 1(a) (dashed black line); harmonics amplitude remains the same while the amplitude of the fundamental is attenuated.

reference signal $v_{\mathrm{ref}}(t)$ is created in a post processing procedure by scaling $v_{\mathrm{lin}}(t)$ to the amplitude of $v_A(t)$ by the amplification factor $k=A/A_{\mathrm{lin}}=5$.

Figure 1(a) shows the superposition of $v_{\mathrm{ref}}(t)$ (solid line) and $v_A(t)$ (dotted line). Nonlinear attenuation and phase shift are present in the signal at the larger amplitude. By subtracting the two signals we obtain the SSM signal $w_A(t)$, which is also reported in Fig. 1(a). Note that $w_A(t)$ has the same content of higher harmonics as $v_A(t)$, while the fundamental one, even if it has been largely reduced [Fig. 1(b)], is still present and dominant. The emergence of higher-order harmonics here is detectable from the deformation of the shape of the signal $w_A(t)$ in Fig. 1(a).

Figures 2(a) and 2(b) show, respectively, the superposition of the signals $v'_A(t)$ and $v''_A(t)$ (dotted lines) on the reference signal (solid line). The agreement of the experimental results with the expectations described in Sec. II C is remarkable.

The contributions $w_1(t)$, $w_2(t)$, and $w_3(t)$ are reported in Figs. 2(c)–2(e). It is clear that $w_1(t)$ and $w_2(t)$ are dominant with respect to $w_3(t)$: the latter is only about 2% of the signal recorded at the larger amplitude. The amplitude of the SSM signal [Fig. 1(a)] is higher than that of the signal in Fig. 2(e), which corresponds to the pure contribution of higher-order harmonics, thus demonstrating the SSM signal to be a richer and more reliable signature of nonlinearity than the filtered signals. Further discussion about this issue will be presented also in Sec. III.

Finally, as expected, the SSM signal $w(t)$ can be reconstructed by the summation of the three independent contributions: $w_R(t)=w_1(t)+w_2(t)+w_3(t)$. Figure 3 shows that the recalculated total signal $w_R(t)$ matches well the measured signal $w_A(t)$. Zooming in a small time window to better appreciate the signals waveform, we notice no significant differences between the two.

## III. EXPERIMENTS

A set of experiments has been conducted to demonstrate the efficiency of the scaling subtraction method for the detection of specimens' nonlinearity through ultrasonic measurements. In addition, experiments have been performed to illustrate the sensitivity of the four SSM signals to the presence and progression of microdamage.

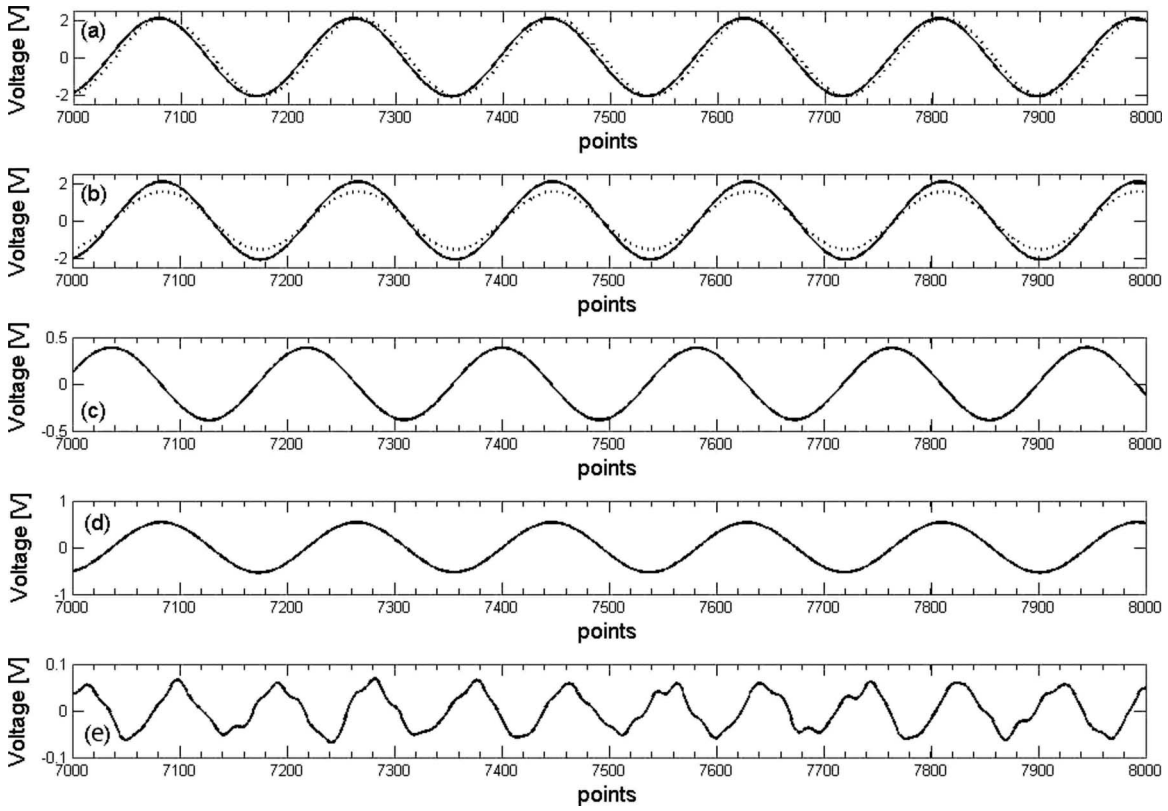


FIG. 2. The SSM contributions. (a) Solid line is the reference linear signal $v_{\mathrm{ref}}$ and dotted line is the scaled nonlinear signal $v'_A(t)$. Notice that signals have the same amplitude but a difference in phase. (b) Solid line is the reference linear signal $v_{\mathrm{ref}}$ and dotted line is the phased nonlinear signal $v''_A(t)$. Signals have here the same phase, but a difference in amplitude. (c) Phase contribution signal $w_1$, given by the difference of the signals in subplot (a). (d) Nonlinear attenuation contribution $w_2$, given by the difference of the signals in subplot (b). (e) Harmonic contribution $w_3$, given by filtering the nonlinear signal $v_A$ excluding the fundamental frequency. Notice that its magnitude is very small if compared to signals in plots (c) and (d). All data are experimental data taken on a mortar sample.

### A. Experimental setup

In our study, linear (steel and lead) and nonlinear (concrete and mortar) samples have been characterized using the SSM approach. All samples, except for mortar, were in the shape of a 16 cm cylinder with 6 cm diameter. Mortar samples were in the shape of a $4\times4\times16$ cm$^3$ prisms. All samples have been tested in their undamaged state. Also, one mortar sample has been damaged with a quasistatic compression load along its maximum dimension, using a servo-controlled mechanical testing system (MTS), and ultrasonic measurements have been performed with the specimen under loading at different loading levels.

To perform ultrasonic measurements, each sample has been equipped with two identical piezoelectric transducers,

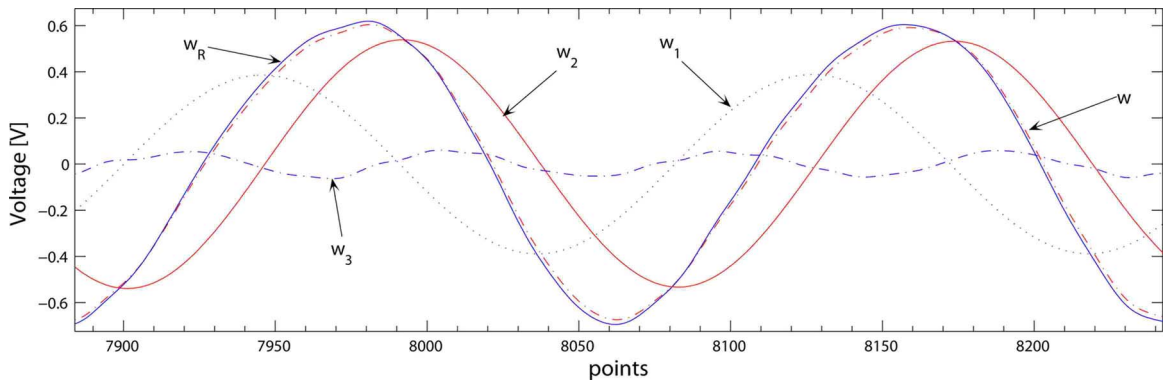


FIG. 3. (Color online) Reconstruction of the SSM signal. The red dashed-dot line is the total SSM signal $w$ ; the blue solid line is the reconstructed SSM signal $w_R$; the blue dotted line is the phase signal $w_1$; the red solid line is the nonlinear attenuation signal $w_2$ contribution and the blue dashed-dot line is the harmonics signal $w_3$. The reconstructed total SSM signal $w_R$ is given by the summation of the $w_1$, $w_2$, and $w_3$ signals and it well corresponds to $w$.

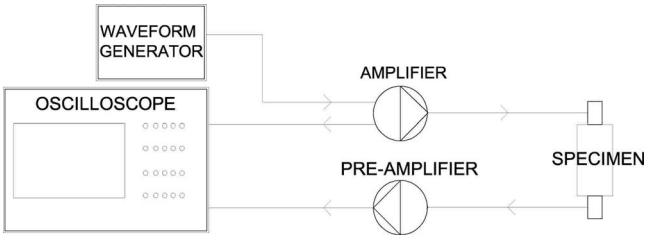


FIG. 4. Schematic representation of the experimental setup. One of the oscilloscope channels measures the output of the power amplifier for synchronization purposes.

one acting as emitter and the other as receiver, with diameter of 4 cm. In the first experiment, transducers have been coupled to the tips of the specimen with a thin layer of plasticine. It follows that the distance between transducers is 16 cm in both cylindrical and prismatic samples. The quality (and linearity) of the bonding and the repeatability of measurements have been verified. In the second experiment, transducers were placed on the sides of the specimen for measurements under loading.

The emitter was connected to a function generator through a linear amplifier; the function generator excited the transducer with a continuous sinusoidal wave centered at frequency $\omega_0=55$ kHz. In the case of measurements under loading, because of the shorter distance available between transducers (4 cm), a higher frequency was chosen: $\omega_0=165$ kHz. The linear amplifier had a 20× gain and made it possible to reach excitations up to 160 V peak to peak.

The amplifier's output was connected to the oscilloscope in order to record and use the input signal to synchronize signals. The receiving transducer was connected to the oscilloscope as well, through a linear preamplifier. Signals have been recorded after stationary conditions were reached, with a sampling rate of 5 MSa/s and a time window of 500 $\mu$s (around 30 wavelengths). See Fig. 4 for a schematic representation of the experimental setup.

For each sample, experiments have been conducted varying the amplitude of the excitation between 2 and 160 V peak to peak, after amplification, with increasing voltage levels and for a total number of $N$ steps. The recorded output signals have been labeled as $v_i$, where $i=1,2,\ldots,N$. The $v_1$ signal is the lower voltage level signal and it corresponds to the linear output signal previously named $v_{\text{lin}}$, while signals from $v_2$ to $v_N$ correspond to the nonlinear responses at different input amplitudes, each of them corresponding to the nonlinear signal $v_A$.

### B. Data analysis

The output signals for ultrasonic measurements, both in unloaded and under loading conditions, have been synchronized and recorded. For each specimen, signal analysis as described in Sec. II made it possible to calculate the total SSM signal $w(t)$ and the partial contributions $w_i(t)$ at each voltage level. For each sample, the nonlinear indicators [the one defined by Eq. (7) and the ones corresponding to the partial contributions] were calculated and plotted as a function of amplitude. In the case of unloaded (and undamaged) specimens, a curve of $\theta$ versus the output signal amplitude was built for each sample. For the loaded progressively damaged mortar specimen, a set of curves, each proper to a specific loading step, was defined.

An increase in the nonlinear indicator as a function of amplitude is characteristic of samples with marked nonlinearity, as discussed below. A faster rate of increase indicates a stronger nonlinearity in the corresponding sample. The curves obtained from the experimental data have been fitted using polynomial equations. In the following, each plot shows both experimental data and fitting curves. The polynomial fitting in this context does not have a physical meaning. Rather it constitutes a guide to the eyes and allows extrapolating the values of the parameters $\theta$ and $\theta_i$ for amplitude values different than those at which experiments have been performed.

### C. Results

#### *1. Unloaded specimens*

As introduced in Sec. III A., two linear (steel and lead) and two nonlinear (mortar and concrete) unloaded specimens have been tested, with the aim of enlightening the efficiency of SSM in characterization of materials. Appropriate measurements on the equipment have been conducted too, in order to ensure linearity of the ultrasonic testing system. In particular, the same procedure followed for the four specimens has been applied to directly coupled transducers, i.e., without interposition of any propagation medium, except for the plasticine layer.

Let us first consider the total nonlinear signature of the four specimens. Figure 5(a) reports the plot of $\theta$ versus the output amplitude of the $v_i$ signals. Linear and nonlinear behaviors can be distinguished. In particular, nonlinear signatures of lead (triangle—black line) and steel (diamond—green line) are negligible if compared to those of mortar (square—red line) and concrete (circle—blue line). The equipment (star—brown line) has a perfectly linear behavior as well. Regarding mortar and concrete, a nonlinear signature is evident and both samples show a nonlinear dependence of $\theta$ from the output amplitude.

Considering the partial contributions and the corresponding indicators, i.e., phase ($\theta_1$), nonlinear attenuation ($\theta_2$), and harmonics content ($\theta_3$), the above observations are still valid. Notice that the harmonics contribution [Fig. 5(d)] is negligible if compared to the contributions of phase and nonlinear attenuation; in particular its magnitude is one order lower than that of the attenuation contribution and two orders lower than phase and total contributions, although it is still clearly distinguishable the nonlinear from the linear behavior. The set of results presented seems to indicate that most of the nonlinear signature resides in the phase mechanism, hence being related to the dependence of the elastic constants from amplitude.

#### *2. Damaged specimen*

We intend here to highlight the efficiency of the SSM method in the detection of variations in nonlinear features in

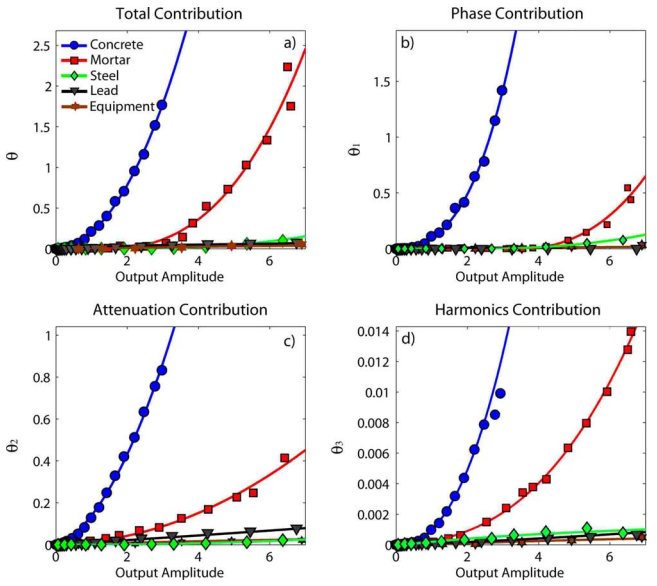


FIG. 5. (Color online) Classification of different specimens by means of their nonlinear signature through the SSM nonlinear indicators ($\theta$ and $\theta_i$ versus output amplitude). (a) The total SSM contribution shows clear distinction between linear (diamonds-green, triangles-black, and stars-brown lines) and nonlinear (squares-red and circles-blue lines) specimens. (b) Phase contribution seems to play a dominant role only for concrete. (c) Nonlinear attenuation shows clear distinction between linear and nonlinear specimens. (d) Harmonics content is sensitive to the nonlinearity of specimens, though its energy content is lower that that of the other contributions (note the different scales on the $y$ axes).

a specimen and thus in the analysis of damage progression. To this purpose, a mortar sample has been damaged through a servo-controlled MTS. Compressive load was increased in steps of 3 kN until rupture occurred, at 38 kN. The MTS worked in displacement control and with a loading velocity of 0.2 $\mu$m/s. Ultrasonic measurements were performed at every loading step, leaving the sample under constant loading condition.

First, we will consider the mechanical behavior of the specimen through the analysis of the quasistatic loading curve. Figure 6 shows a quasistatic curve related to a mortar specimen nearly identical to the one analyzed in the ultrasonic testing: indeed, it has been produced using the very same mixing, in the same day and with the same geometry and size. The analysis of the quasistatic curve shows a compaction stage (hardening), followed by a linear behavior and a nonlinear softening. Rupture occurs at the end of the nonlinear softening stage, at 35 kN.

For the sample investigated with the SSM approach, ultrasonic measurements have been taken in the time interval between one loading step and the following. Figure 7 shows the results of the SSM analysis of the recorded signals $v_i$. The different colored curves represent the total and partial contributions at different loading steps.

Let us first consider the total SSM contribution [Fig. 7(a)]. The curve of the nonlinear parameter $\theta$ does not show a monotonous behavior. At first, a decrease in the nonlinear content in the analyzed signals is manifested (circle-blue and

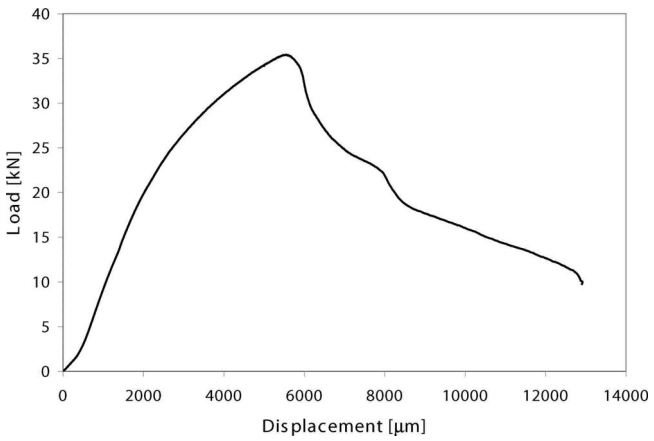


FIG. 6. Quasistatic loading curve for a mortar sample recorded by the acquisition system of the MTS working in displacement control and at a loading velocity of 0.2 $\mu$m/s. Notice the three stages of hardening (slope increase up to 8kN), quasilinearity (constant slope up to 14kN), and damage (slope rapidly decreases up to 33kN). Rupture of the sample occurred at 35 kN.

square-red curves). For higher loads $\theta$ returns to the same values as those of the virgin sample (diamond-green curve), with a very similar behavior. For even larger loads, $\theta$ increases further (stars-yellow and triangles-brown curves). A

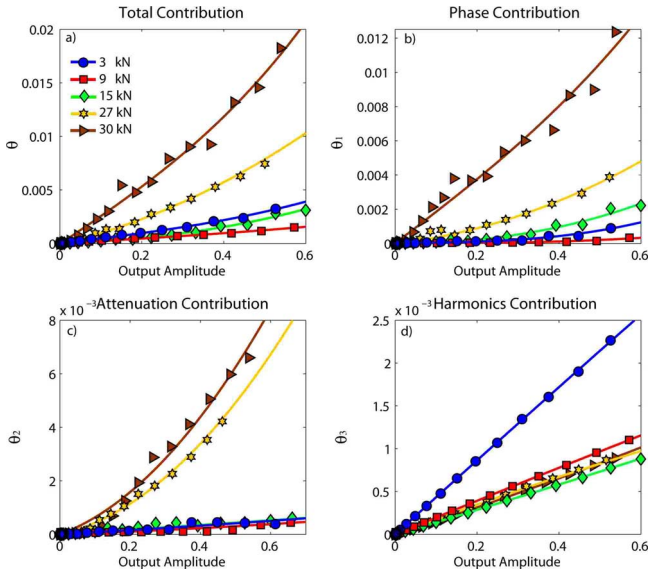


FIG. 7. (Color online) Damage progression in a mortar specimen under quasistatic load. (a) The total SSM indicator highlights three stages: hardening (the nonlinear parameter decreases up to a load of 9 kN), quasilinear elastic region (the nonlinear parameter remains approximately constant up to 20kN: the lines corresponding to 12 and 18 kN, not reported, are very similar to that at 15kN), and softening caused by damage (the nonlinear parameter is larger for 27 and 30 kN). (b) Phase indicator is a magnifying lens on the bulk modulus variations and the hardening stage is very evident. (c) Nonlinear attenuation does not discern the hardening stage, though it shows damage. (d) Harmonics content shows a first decrease in nonlinearity, corresponding to closure of existing cracks in the sample, but it is not sensitive either to hardening or to softening stages.

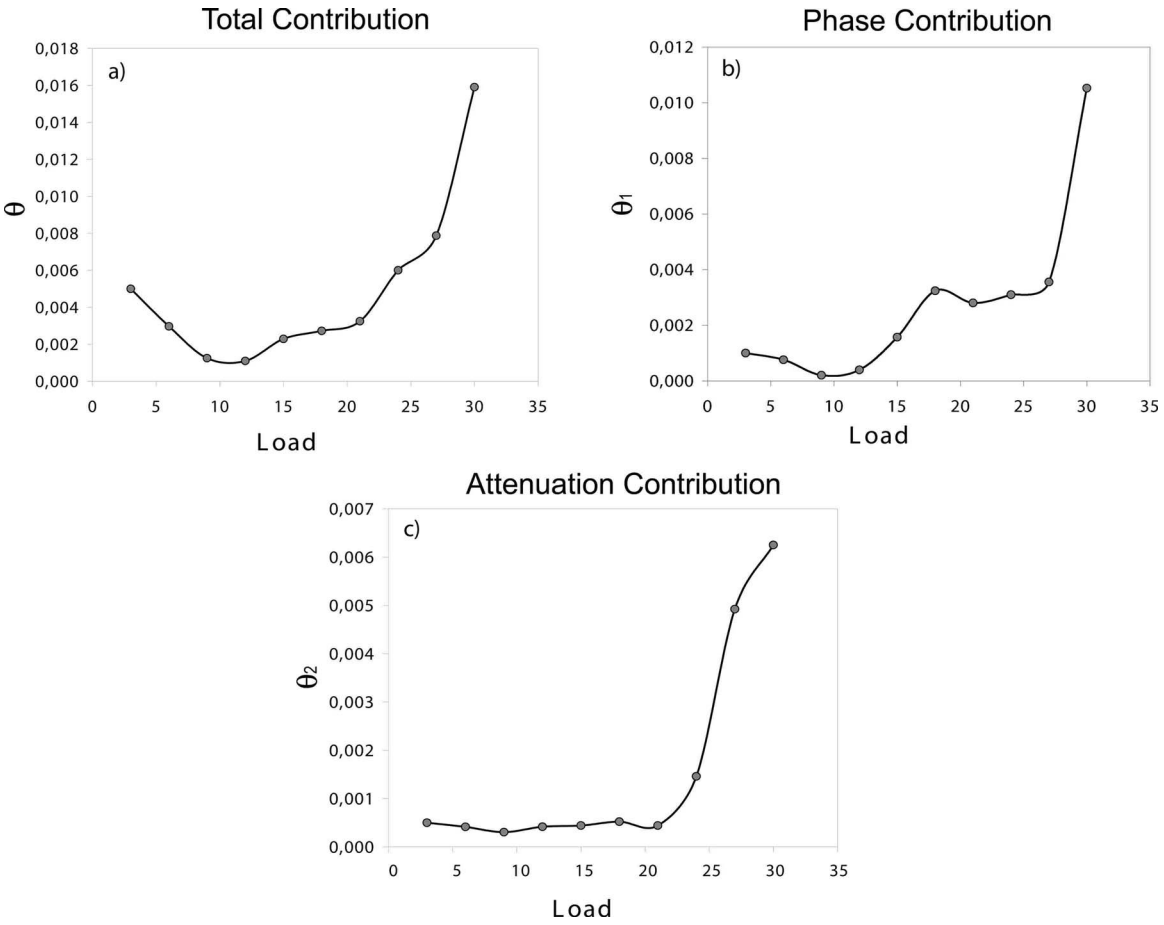


FIG. 8. SSM nonlinear indicators versus load, calculated as discussed in the text. (a) The total nonlinear contribution shows a first decrease, corresponding to the hardening stage. For loading steps between 7 and 21 kN the nonlinear signature may be considered as constant, while a significant increase can be seen from 24 kN to failure. (b) The phase nonlinear signature is very sensitive to changes in the bulk modulus, as well as to the hardening and softening stages. (c) Nonlinear attenuation signature is not sensitive to the hardening stage, although it is very receptive to late damage.

similar observation is also valid for the phase contribution [Fig. 7(b)] and for the nonlinear attenuation indicator [Fig. 7(c)], although the latter seems to be less sensitive to changes up to loads close to 50%–60% of the rupture load. On the contrary, the harmonics content contribution [Fig. 7(d)] does not seem to give any useful information, either for the hardening stage or for the progression of damage. From the second load level on, all curves group in one indistinguishable sheaf. This observation is due to the fact that the harmonics amplitude is very small and probably within the noise level. Notice also the major role played by the phase, enlightened by the higher magnitude of the corresponding indicator.

As the nonlinear signature is related to the presence of microcracks, and thus to damage, it may be useful to cross-analyze results from the quasistatic curve and from the ultrasonic measurements. To this purpose Fig. 8 shows the value of $\theta$ at a fixed output level versus the load. The $\theta$ parameter corresponding to the arbitrarily chosen output level was calculated through the fitting equations. A fixed output amplitude value of 0.4 V was chosen. Although not shown here, no relevant differences in the behavior of the indicators were found for other choices of this value.

The quasistatic curve (reported in Fig. 6) suggests an interpretation of the evolution of the sample microstructure when increasing the load, which is confirmed by the ultrasonic measurements (Fig. 8). In fact, three stages can be distinguished, depending on the concavity of the stress-strain curve.

At first, in correspondence of low load levels, an increase in the slope of the stress-strain curve (upward concavity) highlights that hardening is taking place. In fact, several studies[29–31] have shown that a compaction phase initially occurs when mortar or concrete specimens are stressed with compressive static or cyclic loads. A rearrangement of the internal structure takes place, with microstructures collapsing and pores closing down, which causes a temporary increase in stiffness and, of course, in the bulk modulus. The closure of pre-existing microcracks, not accompanied by formation of new microcracks, leads to a reduction in the nonlinearity of the sample, which is very well captured by the total and phase indicators [Figs. 8(a) and 8(b)] in the range up to 7 kN (about 20% of the rupture load). On the contrary, nonlinearity due to attenuation is not sensitive to compaction.

Then the stress-strain curve indicates a second stage, which can be identified as quasilinear elastic: no significant

changes in the specimen's stiffness occur between 15% and 30% of the rupture load (6 to 12 kN in Fig. 6). Only a few new microcracks are expected to be generated inside the sample. This region is again well captured from the ultrasonic measurements [Figs. 8(a) and 8(b)], the nonlinear indicators being approximately constant in the range 7–12 kN (20%–30% of the rupture load).

When nearly 30% of the maximum compressive strength is reached, the slope of the stress-strain curve begins to gradually decrease (softening downward concavity in the stress-strain relation) and a nonlinear region can be distinguished. A decrease in slope is related to a decrease in the bulk modulus due to the progression of damage caused by the load. Again, the increase in the nonlinear behavior of the sample is captured by the measured nonlinearity indicators. The phase indicator [Fig. 8(b)] is the most sensitive to the very early stages of damage progression (12 kN to 21 kN), while the nonlinear attenuation indicator [Fig. 8(c)] detects an increase in nonlinearity only close to rupture (from 25 kN on, i.e., after having reached 75% of the rupture load).

The data reported in Fig. 8 seem to indicate that the nonlinear indicator $\theta_1$ is sensitive to the stages in which microcracks' density is changing (compaction and early stages of damage progression). Therefore we can expect that early damage will only produce a nonlinear dependence of the elastic constants of the sample and not nonlinear attenuation. In fact, the indicator $\theta_2$ does change only when microcracks are probably coalescing into macrocracks (large loading levels). In other words, it seems that in mortar the nonlinearity in the attenuation is mostly dominated by the presence of large damage regions, rather than from the opening of microcracks in the material.

Concluding this section, we remark that changes in the phase and attenuation at the fundamental frequency correspond to a dependence on amplitude of the resonance curve of the sample, as studied elsewhere.[1,3,10,20–24] In fact, both the resonance frequency shift and the phase dependence on amplitude are linked to a velocity variation in the waves in the medium. Also, the changes in the $Q$ factor of the sample with amplitude can be extracted from resonance measurements with an often complex mathematical approach. In our opinion, the approach presented here is faster and easier than resonance measurements.

### D. Comparison with other techniques

As mentioned in Sec. I, other methods for the analysis of the data can be used to classify the elastic nonlinearity of the sample based on its response to an ultrasonic excitation. Among them, the strain dependence of the harmonics amplitude and of the phase delay provide information about the classical parameters $\beta$ and $\delta$. In particular, assuming a power-law dependence in the form

$$y = ax^b, \tag{11}$$

the type of nonlinearity can be identified from the exponents $b$ calculated for the second harmonic, third harmonic, and phase delay dependence on the amplitude of the fundamental harmonic ($x$). In particular, for a completely hysteretic system, we expect the exponent $b$ to be equal to 2 for both second- and third-harmonic dependences and to be equal to 1 for the phase delay.

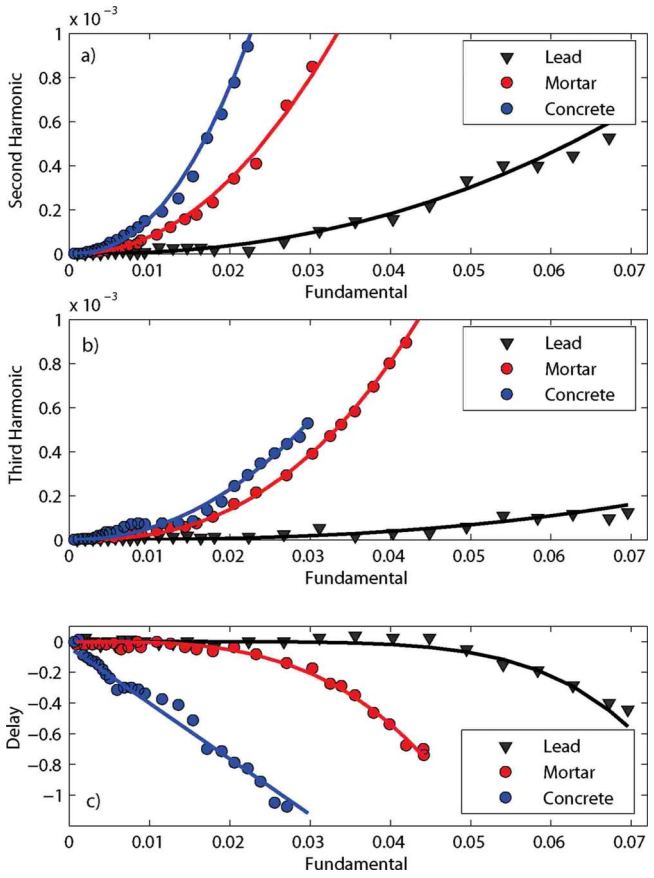


FIG. 9. (Color online) Strain dependence of (a) the second-harmonic amplitude, (b) the third harmonic amplitude, and (c) the phase delay (c) for different materials. The power-law dependence (solid lines are the fitting curves) indicates a small classical nonlinearity for lead, a combination of classical and hysteretic nonlinearity for mortar, and a dominant hysteric nonlinearity for concrete. Exponents of the power-law dependence are reported in the text.

We have applied this analysis to the data presented in Sec. III C 1 (unloaded samples). The amplitudes of the second [Fig. 9(a)] and third harmonics [Fig. 9(b)] are reported vs the amplitude of the fundamental in the cases of lead, mortar, and concrete (the experimental data correspond to symbols in the figure). The phase delay is reported in Fig. 9(c). A fit with a power law (solid line in the figure) provided the following exponents:

(i) lead: $b=2.28$ (second harmonic); $b=2.97$ (third harmonic); $b=6$ (phase delay). The very small coefficients $a$ and the exponents found indicate a weak classical nonlinearity;

(ii) mortar: $b=2.12$ (second harmonic); $b=2.57$ (third harmonic); $b=3$ (phase delay). The coefficients $a$ are significant and the exponents found indicate a combination of classical and hysteretic nonlinearity;

(iii) concrete: $b=2.26$ (second harmonic); $b=2.12$ (third harmonic); $b=1.02$ (phase delay). The coefficients $a$ are large and the exponents found indicate a dominant hysteretic nonlinearity.

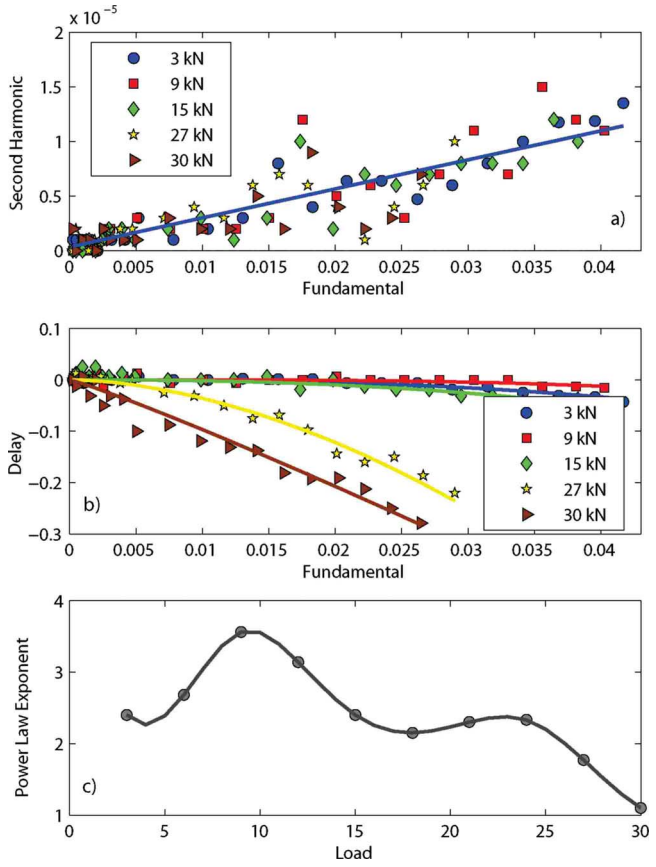


FIG. 10. (Color online) Strain dependence of (a) the second-harmonic amplitude and (b) the phase delay for the mortar sample at different load levels. The linear dependence of the second-harmonic amplitude indicates that harmonics fall within the noise level. The exponents for the power-law dependence for the phase delay [solid lines in subplot (b) are the fitting curves] are reported vs load level in subplot (c). Compare the results with Fig. 8(b).

More complex is the case of the under load experiment (Sec. III C 2). Here, the frequency chosen is $\omega_o = 165$ KHz and measurements are noisier due to the action of the MTS machine, working during the ultrasonic measurements to keep the load on the sample. Therefore, we expect the analysis of the harmonics to be harder, both because of the decreased signal-to-noise ratio and because of the bandwidth of the transducers. Indeed, as reported in Fig. 10(a), the second harmonic depends linearly from the fundamental one, with no differences at the various loading levels, thus indicating that their amplitudes fall within the noise level and cannot be used for the characterization (a similar behavior is found also for the third harmonic). On the contrary, the phase delay [Fig. 10(b)] can still be appreciated and its dependence from the strain amplitude is different at the various loadings. In particular, the exponent $b$ can be plotted vs load [Fig. 10(c)]. We found a result very similar to that of Fig. 8(b), although the quality of the results is not as good. It is interesting to observe that, approaching the rupture load (37 kN), nonlinearity of the sample seems to approach an hysteretic dependence ($b=1$).

## IV. DISCUSSION

The experimental results reported so far (and others, not reported for brevity) show that the phase indicator $\theta_1$ is generally the most suitable to pin point the nonlinearity of the sample. For instance, Fig. 8 shows that $\theta_1$ is sensitive to both compaction and damage progression in a sample subject to quasistatic loading. Also, during the setup of the experiments, we have noticed that the phase indicator is much less sensitive to the experimental setup than the other indicators, with easier reproducibility under less controlled experimental procedures.

We indicate here two possible interpretations of the results obtained. The first is that $\theta_1$ is sensitive to the dependence of the wave speed from amplitude, i.e., to variations in the elastic constants of the sample. Since we do not consider changes in amplitude, but only in phase, effects due to changes in the resonance frequency of the sample, which can make complex the interpretation of the full SSM signal ($\theta$ indicator), are automatically filtered out. Also, the dependence of the elastic constants from amplitude is probably the most common cause of nonlinearity in the samples considered.

A second consideration is that the phase contribution automatically filters out imperfections due to the transducers and coupling medium. To demonstrate this item, we have performed a set of numerical experiments, using a two-dimensional (2D) code for the description of the propagation of elastic waves in nonlinear solid media based on the spring model approach.[21,32–34] We have considered an aluminum rectangular sample (20 cm by 10 cm) with a square nonlinear inclusion centered in $x=3.0$ cm, $y=4.2$ cm (with size 1.0 cm by 0.5 cm). A transducer has been located in $x=0.0$ cm, $y=5.0$ cm, injecting different kind of pulses, as detailed below. 26 receivers have been located at various distances from the source, and the nonlinearity indicators defined previously have been calculated from the signals recorded at the different positions. The ratio $A_{\text{nonlin}}/A_{\text{lin}}=10$ (ratio between the large and low amplitudes of the signals injected in the simulation) has been used, but results are qualitatively independent from this ratio. Also, we have shown that the considerations reported in the following are valid for different defect sizes and for an extended nonlinearity (i.e., distributed in the full sample).

To characterize different forms of imperfections at the transducer (either due to coupling or due to the transducer nonlinearity), we have considered three typical cases. In each of them we have assumed the signal injected from the generator to be a Gaussian modulated cosine pulse with central frequency $\omega_0$,

$$f(t) = A\cos[\omega_0(t-t_0)]e^{-(t-t_0)^2/2\sigma^2}. \tag{12}$$

The width is $\sigma = 2/\omega_0$ such that the injected signal does not contain frequencies multiple of $\omega_0$.

We have assumed the signal $f(t)$ to be distorted to a signal $f'(t)$ before injection as follows, for the three cases:

(1) perfect transducer: we assume the transducer injects exactly what is expected: $f'(t)=f(t)$;

(2) short-time pulse transducer: we assume the transducer induces time compression of the signal. Therefore $f'(t)$ is the same as $f(t)$ except that $\sigma=0.5/\omega_0$ such that the injected signal contains already frequencies multiple of $\omega_0$. Note that short-time signals are often chosen directly at the generator since they are more suitable in several situations;

(3) nonlinear transducer: we assume the equipment has an intrinsic nonlinearity so that distortions introduce nonlinear terms with random amplitudes. Also, an instability in the amplitude at the fundamental frequency is considered,

$$f'(t) = \{A_1 \cos[\omega_0(t-t_0)] + A_2 \cos[2\omega_0(t-t_0)] + A_3 \cos[3\omega_0(t-t_0)]\} e^{-(t-t_0)^2/2\sigma^2}. \quad (13)$$

Since we are interested in small distortions, the three random amplitudes $A_i$ have been chosen such that $A_1$ deviates at most of ten percent from $A$, while $A_2$ and $A_3$ are at most 10 percent and 5 percent of $A$. It is important to note that, to simulate a realistic condition, for each experiment (i.e., each amplitude of injection) the random amplitudes have been generated independently.

For each transducer we have estimated the nonlinear indicators in a linear (without the inclusion) and a nonlinear (with the inclusion) sample. The nonlinear indicators are reported in Figs. 11 and 12 for the various cases as a function of the distance from the source. As expected, all indicators allow distinguishing the nonlinear from the linear sample when a perfect transducer is used (black circles and white squares in Fig. 11). On the contrary, when a short-time transducer is used, the harmonic indicator $\theta_3$ is of the same order of magnitude for both the linear (yellow squares) and the nonlinear (red diamonds) samples: see Fig. 11(c). It follows that a defect in the source can be erroneously interpreted as a nonlinearity of the sample.

The situation is even worse if a nonlinear transducer is considered (Fig. 12). Here, the indicator $\theta$, related to the full SSM signal, is the same for linear and nonlinear samples [Fig. 12(a)], due to the impossibility to normalize correctly the low and large amplitude signals, being random the amplitude at the injection. Also the harmonics indicator, reported in Fig. 12(c), does not allow separating clearly the behavior of the linear sample (yellow squares) from those of the nonlinear samples (black circles and red diamonds). In particular, a receiver located far from the source can detect the same amount of harmonics for a nonlinear sample than a receiver located close to the source but in a linear sample.

Figures 11(b) and 12(b) show that the phase indicator $\theta_1$ is capable to distinguish a nonlinear sample from a linear one, independently from the receiver position and from the transducer imperfections. It is to be noted that the advantages of the phase indicator with respect to the other two are not always evident and strongly depend on the ratio between the nonlinearity amplitude (or extension) and the transducer level of imperfection. Nevertheless, from the several cases analyzed we can state that $\theta_1$ is always as good as, or better than, the other two.

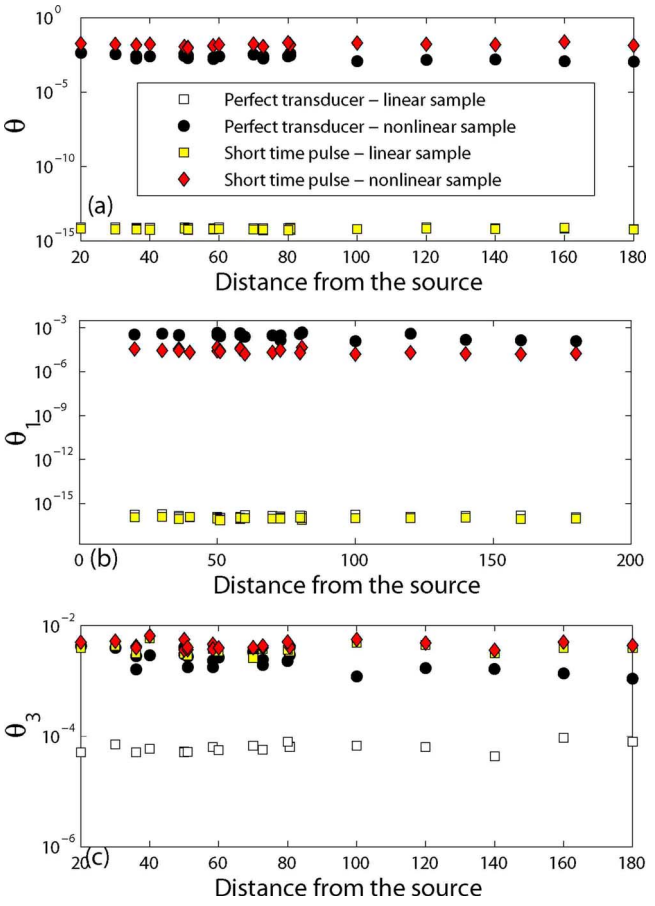


FIG. 11. (Color online) Nonlinear indicators as a function of the distance of the detecting receiver from the source calculated from different numerical experiments: perfect and short-time pulse transducers injecting in a linear sample (squares) or in a linear sample with a small nonlinear inclusion (circles and diamonds). (a) total SSM indicator; (b) phase indicator; (c) harmonics indicator.

## V. CONCLUSIONS

We have shown in this paper how information about the elastic nonlinearity of a sample can be extracted using a scaling subtraction method (SSM) as an alternative to traditional filtering or FFT analysis. Using the proposed subtraction procedure, we have identified three nonlinear indicators, which identify, each of them, one specific consequence of the nonlinearity of the sample: dependence of the elastic constants on amplitude, dependence of attenuation on amplitude, and harmonics generation. Each of them, together with the indicator considering the three contributions together, can provide specific information on the nonlinearity of the system and can find useful applications in different problems.

The method has been validated experimentally and we have shown the sensitivity of SSM to detect compaction and damage progression in specimens (mortar) subjected to quasistatic loading. The results reported here are in agreement with other studies on concrete samples, performed without the separation of the three contributions[11] and confirm the difficulties of extracting information on damage progression in structural materials with the use of harmonics only.[35] Indeed, the indicator proposed connected to the phases of the

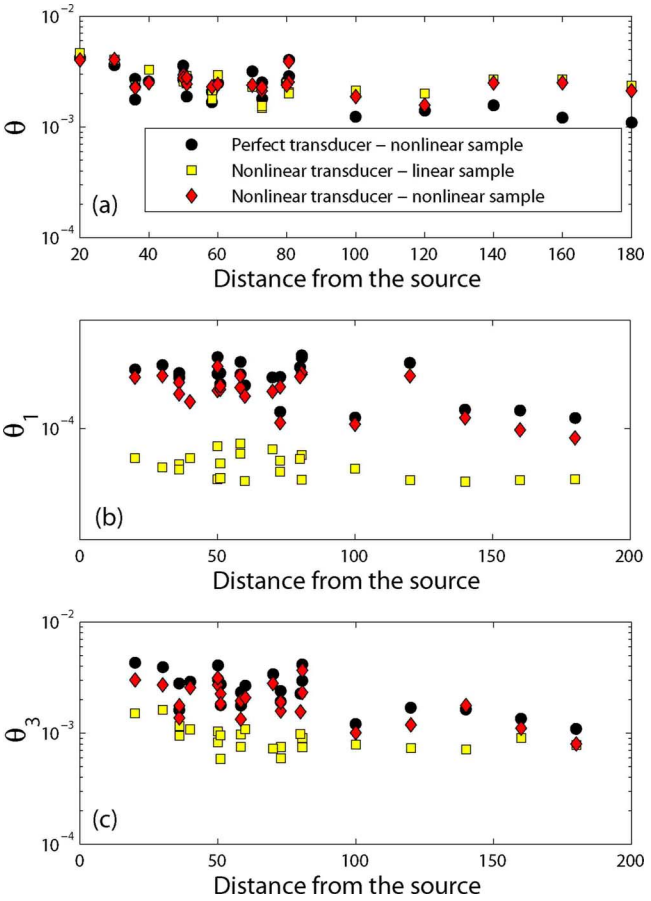


FIG. 12. (Color online) Nonlinear indicators as a function of the distance of the detecting receiver from the source calculated from different numerical experiments: nonlinear transducer injecting in a linear sample (squares) or in a linear sample with a small nonlinear inclusion (diamonds). Results for a perfect transducer injecting in a nonlinear sample are also reported (circles, same as in Fig. 9). (a) total SSM indicator; (b) phase indicator; (c) harmonics indicator

signals seems to us to be the most promising in view of applications, either in the field of nondestructive evaluation or nonlinear time-reversal acoustics.[36] In fact, it is possible to separate the nonlinear contributions of the sample from those due to transducers and equipment imperfections.

## APPENDIX

The scaling subtraction method is based on the definition of a reference signal $v_{\mathrm{ref}}(t)$, which satisfies a linear equation

$$\ddot{v}_{\mathrm{ref}} = c_l^2 v'', \tag{14}$$

where a dot indicates a time derivative, a prime a space derivative and $c_l$ is the longitudinal wave velocity of the investigated sample. Likewise, a second (large amplitude) signal $v_A(t)$ is defined, which satisfies the nonlinear equation governing the wave propagation in the sample. For sake of simplicity, in this example we consider a simple nonlinear model, based on a second-order expansion of the elastic constants in terms of strain.[26] The following equation holds:

$$\ddot{v}_A = c_l^2 (v_A'' + \beta v_A' v_A''). \tag{15}$$

Simple calculations show that the scaled subtracted signal

$$w_A(t) = v_A(t) - v_{\mathrm{ref}}(t) \tag{16}$$

must satisfy the following differential equation:

$$\ddot{w}_A = c_l^2 (w_A'' + \beta w_A' w_A'') - \beta c_l^2 [v_{\mathrm{ref}}' w_A'' - (v_{\mathrm{ref}}' + w_A') v_{\mathrm{ref}}']. \tag{17}$$

Assuming the signal $w_A(t)$ small (i.e., of the same order of magnitude as $\beta$), we can neglect the nonlinear term in $w_A(t)$. Furthermore, being the reference signal $v_{\mathrm{ref}}(t)$ solution of the linear propagation equation, it can be written as

$$v_{\mathrm{ref}}(t) = B \cos(kx + \omega t), \tag{18}$$

$$k = c_l \omega; \quad B = k A_{\mathrm{lin}}. \tag{19}$$

Therefore, the signal $w_A(t)$ satisfies a linear nonhomogenous differential equation, which can be solved. We adopt a perturbative treatment similar to that adopted in Refs. 37 and 38. We seek a solution perturbatively as

$$w_A(t) = x_0 \cos(kx + \omega_0 t) + \beta w_{A,1} + \beta^2 w_{A,2} + \cdots. \tag{20}$$

The first-order solution gives us

$$w_{A,1} = (y_0 + y_1 t) \cos(2kx + 2\omega_0 t), \tag{21}$$

$$y_1 = -\frac{k^2 \sqrt{c_l}}{8} A_0^2. \tag{22}$$

To perform a quantitative comparison between the SSM nonlinear indicator $\theta$ and the "classical" nonlinear parameter $\beta$, further terms in the expansions and attenuation must be included in the analysis. Furthermore, Eq. (17) must be solved with the appropriate boundary conditions for a finite sample. This is, in our opinion, beyond the scope of the present paper since our samples cannot be described in the framework of classical nonlinear models.

*caterina.bruno@polito.it
†antonio.gliozzi@polito.it
‡marco.scalerandi@infm.polito.it
§paola.antonaci@polito.it

[1] R. A. Guyer and P. A. Johnson, Phys. Today **52**, 30 (1999).
[2] P. B. Nagy, Ultrasonics **36**, 375 (1998).
[3] K. Van den Abeele, P. A. Johnson, and A. Sutin, Res. Nondestruct. Eval. **12**, 17 (2000); X. J. Chen, J. Y. Kim, K. E. Kurtis, J. Qu, C. W. Shen, and L. J. Jacobs, NDT & E Int. **41**, 112 (2008).
[4] J. Herrmann, J.-Y. Kim, and L. J. Jacobs, J. Appl. Phys. **99**, 124913 (2006).

[5] M. X. Deng and J. F. Pei, Appl. Phys. Lett. **90**, 121902 (2007).
[6] I. Solodov, J. Wackerl, K. Pfleiderer, and G. Busse, Appl. Phys. Lett. **84**, 5386 (2004).
[7] K. Van den Abeele and J. De Vissche, Cement Concr. Res. **30**, 1453 (2000).
[8] A. Moussatov, V. Gusev, and B. Castagnede, Phys. Rev. Lett. **90**, 124301 (2003).
[9] P. Duffour, M. Morbidini, and P. Cawley, J. Acoust. Soc. Am. **119**, 1463 (2006).
[10] P. A. Johnson and A. Sutin, J. Acoust. Soc. Am. **117**, 124 (2005).
[11] M. Scalerandi, A. S. Gliozzi, C. L. E. Bruno, and P. Bocca, Appl. Phys. Lett. **92**, 101912 (2008).
[12] T. J. Ulrich, P. A. Johnson, and R. A. Guyer, Phys. Rev. Lett. **98**, 104301 (2007).
[13] T. Goursolle, S. Callé, S. Dos Santos, and O. Bou Matar, J. Acoust. Soc. Am. **122**, 3220 (2007).
[14] T. J. Ulrich, P. A. Johnson, and A. Sutin, J. Acoust. Soc. Am. **119**, 1514 (2006).
[15] A. S. Gliozzi, M. Griffa, and M. Scalerandi, J. Acoust. Soc. Am. **120**, 2506 (2006).
[16] I. Solodov and G. Busse, Appl. Phys. Lett. **91**, 251910 (2007).
[17] C. Campos-Pozuelo, C. Vanhille, and J. A. Gallego, IEEE Trans. Ultrason. Ferroelectr. Freq. Control **53**, 175 (2006).
[18] T. Goursolle, S. Dos Santos, O. Bou Matar, and S. Callé, Int. J. Non-linear Mech. **43** (3), 170 (2008); M. Vila, F. Vander Meulen, S. Dos Santos, L. Haumesser, and O. Bou Matar, Ultrasonics **42**, 1061 (2004).
[19] L. D. Landau and E. M. Lifshitz, *Theory of elasticity* (Pergamon, Oxford, 1986).
[20] B. Capogrosso-Sansone and R. A. Guyer, Phys. Rev. B **66**, 224101 (2002).
[21] P. P. Delsanto and M. Scalerandi, Phys. Rev. B **68**, 064107 (2003).
[22] M. Nobili and M. Scalerandi, Phys. Rev. B **69**, 104105 (2004).
[23] O. O. Vakhnenko, V. O. Vakhnenko, T. J. Shankland, and J. A. Ten Cate, Phys. Rev. E **70**, 015602(R) (2004).
[24] P. P. Delsanto, S. Hirsekorn, V. Agostini, R. Loparco, and A. Koka, Ultrasonics **40**, 605 (2002).
[25] J.-Y. Kim, A. Baltazar, and S. I. Rokhlin, J. Mech. Phys. Solids **52**, 1911 (2004).
[26] M. Vila, M. F. Meulen, S. Dos Santos, and O. Bou Matar, Ultrasonics **42**, 1061 (2004).
[27] J. A. TenCate, D. Pasqualini, S. Habib, K. Heitmann, D. Higdon, and P. A. Johnson, Phys. Rev. Lett. **93**, 065501 (2004).
[28] V. O. Vakhnenko, O. O. Vakhnenko, J. A. TenCate, and T. J. Shankland, Phys. Rev. B **76**, 184108 (2007).
[29] M. Berra and P. Bocca, Mater. Struct. **26**, 395 (1993).
[30] P. Bocca and P. Antonaci, Cement Concr. Res. **35**, 1776 (2005).
[31] N. Burlion, G. Pijaudier-Cabot, and N. Dahan, Int. J. Numer. Anal. Methods Geomech. **25**, 1467 (2001).
[32] P. P. Delsanto and M. Scalerandi, J. Acoust. Soc. Am. **104**, 2584 (1998).
[33] A. S. Gliozzi, M. Nobili, and M. Scalerandi, J. Phys. D **39**, 3895 (2006).
[34] N. Cretu, P. P. Delsanto, G. Nita, C. Rosca, M. Scalerandi, and I. Sturzu, J. Acoust. Soc. Am. **104**, 57 (1998).
[35] P. Antonaci, P. Bocca, D. Masera, N. Pugno, M. Scalerandi, and F. Sellone, Key Eng. Mater. **347**, 633 (2007).
[36] M. Scalerandi, A. S. Gliozzi, C. L. E. Bruno, and K. Van Den Abeele, J. Phys. D **41**, 215404 (2008).
[37] B. F. Apostol, Phys. Lett. A **318**, 545 (2003).
[38] T. Brunet, X. Jia, and P. A. Johnson, Geophys. Res. Lett. **35**, L19308 (2008).